h-adaptivity and 'honest' GFEM for advection dominated transport

Asif S. Usmani, David A. Mayne and Martin Crapper

School of Civil and Environmental Engineering

The University of Edinburgh

The Kings Buildings

Edinburgh EH9 3JN

United Kingdom

Abbreviated title: ***h*-adaptivity and 'honest' GFEM**

NOMENCLATURE

A	angle of rotation
C_p	specific heat capacity ($m^2\ s^{-2}K^{-1}$)
e	*a-posteriori* error
$\mathbf{F}$	right hand side vector
F	traction force ($kg\ m\ s^{-2}$)
$\mathbf{g}$	acceleration due to gravity ($m\ s^{-2}$)
h_e	element size (m)
k	thermal conductivity ($m\ kg\ s^{-3}$)
$\mathbf{K}$	stiffness matrix
L	characteristic length (m)
m	number of elements
$\mathbf{M}$	consistent mass matrix
$\mathbf{n}$	unit normal vector
Nu	Nusselt number
P	pressure ($kg\ m^{-1}\ s^{-2}$)
$\mathbf{q}$	heat flux ($kg\ s^{-3}$)
Q	smoothed value of total heat flow dissipation ($kg\ s^{-3}$)
$\hat{Q}$	total heat flow dissipation ($kg\ s^{-3}$)
Ra	Rayleigh number
t	time (s)
t^*	non-dimensionalised time
T	dependent scalar variable or temperature
u	velocity in the x - direction ($m\ s^{-1}$)
v	velocity in the y - direction ($m\ s^{-1}$)
v^*	non-dimensionalised velocity in the y - direction
$\mathbf{v}$	velocity vector ($m\ s^{-1}$)
$\mathbf{v_o}$	intial value of the velocity vector ($m\ s^{-1}$)
W	weighting functions

α	time stepping factor
β	volumetric coefficient of thermal expansion
Γ	control surface
ΔT	time step size
η	percentage error
$\bar{\eta}$	maximum permissible percentage error
κ	thermal diffusivity ($m^2\ s^{-1}$)
μ	dynamic viscosity (kg $m^{-1}\ s^{-1}$)
ρ	density of fluid (kg m^{-3})
Ω	domain area (m^2)

ABSTRACT

A standard 2D GFEM code for coupled Navier-Stokes and energy equations is used with h-adaptive meshing based on *a-posteriori* error estimation using the super-convergent patch recovery technique for solving a range of advection dominated transport problems. It is demonstrated that such a method provides a highly effective, simple and efficient way of dealing with the perennial problems in numerical modelling of advection dominated transport, such as oscillations or wiggles with central difference type discretisations (such as GFEM) and numerical ('false') diffusion when wiggle-suppressent schemes are used. Additionally, the auto-adaptive finite element method provides a powerful means of achieving optimal solutions without having to pre-define a mesh, which may be either inadequate or too expensive. A number of benchmark problems are presented as application examples for this method before solving a problem of natural convection in an air filled cavity with various orientations, for which experimental results are available.

1 INTRODUCTION

A lot has been written on the issue of dealing with "wiggles" or oscillations in CFD solutions, generated most commonly when using spatial (or temporal) discretisations akin to central differencing, for instance the Galerkin Finite Element Method often abbreviated to GFEM [1]. The informed opinion on this issue has tended to gravitate towards one of the two groups of protagonists, one favouring the use of 'honest' methods and tolerating wiggles as a 'self diagnostic property' [1] and the other advocating use of special techniques to suppress the wiggles resulting in smoother solutions. In the relatively smaller group of FEM-CFD researchers, the former group is led, quite vociferously, by Phil Gresho and his colleagues [2] and we recognise Thomas Hughes [3], as the foremost member of the latter group (again from a finite element perspective). We have immense respect for both of these authors and their eminent colleagues and have profited abundantly from their labours. One purpose of this paper is to provide a review of our experiences with both of these, ostensibly, opposing philosophies.

One of the principal reasons for generation of wiggles is lack of spatial resolution available in the computational mesh. This is particularly problematic when dealing with advection of wave-forms not adequately resolved by the mesh, as it is advection that really tests the mesh resolution because of much higher signal propagation rate relative to diffusive processes. A detailed analysis of the reasons for this can be be found in [1], among others. If the problem is identified as being that of inadequate spatial resolution, the remedy then simply becomes a matter of exercising care in designing ones mesh. However, this is not a simple task and does to an extent require an *a-priori* knowledge of the solution. Furthermore, in dealing with time-dependent problems, the mesh resolution requirement may change over the course of the analysis, making it even more difficult and expensive to use a single mesh that retains adequate discretisation. These questions naturally lead one to look for a solution based on adaptive mesh refinement strategies as it did one of the authors [4, 5]. This work has been extended considerably over the years [6–8] and a large number of numerical experiments have been undertaken to show that the h-adaptive mesh refinement provides an effective bridge between the two opposing philosophies discussed above. It can be used in conjunction with good Petrov-Galerkin methods (such as SUPG [3]) to provide a solution where it may be impossible to achieve with 'honest' GFEM for 'difficult' problems (such as [5]) and it can be used just with 'honest' GFEM for most advection dominated time-dependent problems with impressive results [9]. In effect this method provides a mechanism whereby an experienced user has the choice of using 'pure' central difference

type discretisations with highly refined adaptive meshes or adding a degree of upwinding with selective refinement to obtain 'smooth' solutions, all the while being aware of the merits or otherwise of their choices.

In the following sections the basic equations and formulations, which are standard and well known, will be reproduced in brief, for completeness. A review of some of the earlier work mentioned above will be undertaken and selected results will be presented. Finally the method (using the author's program CADTRAS Coupled Advective Diffusive TRAnSport model) will be used to solve an experimental benchmark problem by Leong *et al* [10, 11]. They have undertaken experiments to produce a three dimensional thermally driven titling cavity benchmark problem and have also solved it numerically. Nusselt numbers have been made available for various inclination angles and Rayleigh numbers with a view to establishing a physically-realizable benchmark solution for CFD code validation. This paper aims to solve this essentially 3-D problem using a 2-D code and compare results with existing experimental and numerical solutions set out by Leong *et al* [11]. The purpose is to demonstrate, using another example, the effectiveness of the proposed combination of h-adaptivity with 'honest' GFEM.

2 GOVERNING EQUATIONS AND NUMERICAL FORMULATION

For the problems considered in this paper, either a scalar advection-diffusion equation has been solved on its own or it has been solved as part of a coupled set with the Navier-Stokes equations for incompressible flow:

The Navier-Stokes equations with a Boussinesq approximation included for natural convection problems:

$$\rho\left(\frac{\partial \mathbf{v}}{\partial t} + \mathbf{v}\cdot\nabla\mathbf{v}\right) + \nabla P \;=\; \nabla\cdot\mu\left[\nabla\mathbf{v} + (\nabla\mathbf{v})^T\right] - \rho\mathbf{g}\beta\left(T - T_r\right) \quad \texttt{on} \quad \Omega \tag{1}$$

subject to the Continuity constraint:

$$\nabla\cdot\mathbf{v} \;=\; 0 \quad \texttt{on} \quad \Omega \tag{2}$$

These equations are subject to the usual set of boundary conditions:

$$\mathbf{F} \;=\; P\mathbf{n} - \mu\left[\nabla\mathbf{v} + (\nabla\mathbf{v})^T\right]\cdot\mathbf{n} \quad \texttt{on} \quad \Gamma_F \tag{3}$$

$$\mathbf{v} \;=\; \bar{\mathbf{v}}\,(x,y,t) \quad \texttt{on} \quad \Gamma_v \tag{4}$$

and initial conditions:

$$\mathbf{v}\,(t=0) = \mathbf{v_o} \qquad \text{with} \qquad \nabla \cdot \mathbf{v_o} = 0 \tag{5}$$

The notations have commonly implied meanings, therefore, $\mathbf{v}$ represents the velocity, T represents temperature, T_r is a reference temperature, P represents pressure, μ is the dynamic viscosity, $\mathbf{g}$ is the acceleration due to gravity, β is the volumetric coefficient of thermal expansion, $\mathbf{F}$ represents the applied tractions on the boundary Γ_F, n is the unit normal vector and $\bar{\mathbf{v}}$ is the Dirichlet boundary condition for velocity on the part of the boundary Γ_v.

The Scalar Advection-Diffusion equation written using T as the dependent variable:

$$\frac{\partial T}{\partial t} + \mathbf{v} \cdot \nabla T \;=\; \nabla \cdot \kappa \nabla T \quad \texttt{on} \quad \Omega \tag{6}$$

subject to boundary conditions:

$$\mathbf{n} \cdot (\kappa \nabla T) \;=\; q \quad \texttt{on} \quad \Gamma_Q \tag{7}$$

$$T \;=\; \bar{T}\,(x,y,t) \quad \texttt{on} \quad \Gamma_T \tag{8}$$

and initial conditions:

$$T\,(t=0) = T_o \tag{9}$$

where q is a specified normal scalar flux on the boundary Γ_Q, $\bar{T}$ is the specified value of the scalar on the boundary Γ_T and κ is the diffusivity, which for heat transfer problems is given by,

$$\kappa \;=\; \frac{k}{\rho C_p} \tag{10}$$

where, k is the thermal conductivity, ρ is the fluid density and C_p is the specific heat capacity.

2.1 Finite element method

The standard Galerkin form of the finite element method (GFEM) is applied to the equation system using the *mixed* formulation with lower interpolation of pressures than that of the velocities. This method is primarily chosen as it is 'honest' GFEM and with unconditionally stable implicit time integration schemes (such as the mid-point rule used here) it is perfectly suited for use with h-adaptive mesh refinement. The semi-discrete Navier-Stokes and scalar transport equations are presented as follows using notation from Gresho *et al*, [12, 13]:

Navier-Stokes

$$\begin{bmatrix} \mathbf{M_u} & 0 & 0 \\ 0 & 0 & 0 \\ 0 & 0 & \mathbf{M_v} \end{bmatrix} \begin{pmatrix} \dot{\mathbf{u}} \\ \dot{\mathbf{P}} \\ \dot{\mathbf{v}} \end{pmatrix} + \begin{bmatrix} \mathbf{K_{uu}} & \mathbf{C_u} & \mathbf{K_{uv}} \\ \mathbf{C_u^T} & 0 & \mathbf{C_v^T} \\ \mathbf{K_{vu}} & \mathbf{C_v} & \mathbf{K_{vv}} \end{bmatrix} \begin{pmatrix} \mathbf{u} \\ \mathbf{P} \\ \mathbf{v} \end{pmatrix} = \begin{pmatrix} \mathbf{F_u} \\ 0 \\ \mathbf{F_v} \end{pmatrix} \tag{11}$$

Scalar advection-diffusion

$$[\,\mathbf{M_T}\,](\,\dot{\mathbf{T}}\,) + [\,\mathbf{K_T}\,](\,\mathbf{T}\,) = (\,\mathbf{F_T}\,) \tag{12}$$

Where $\mathbf{M}$, $\mathbf{K}$, $\mathbf{C}$ and $\mathbf{F}$ represent the mass matrix, viscous stress matrix, pressure gradient matrix and global force vector respectively. Expansion of all terms can be found in Usmani *et al* [14]. The two systems of equations above are solved as required: either as a coupled system, with the $\mathbf{K_T}$ term containing the velocities (obtained from solving the flow field) and the $\mathbf{F_v}$ term containing the buoyancy forces (determined by the temperature field) for natural convection problems; or separately from each other for a given problem. For the coupled flow and scalar transport problems a six-noded Taylor-Hood [15] element (with 3 continuous pressure nodes) is used, which is not the best choice for enforcing continuity, however it is sufficient for the purposes of this paper. Therefore, the program solves for the primitive variables: u-velocity, v-velocity and T-scalar at all nodes in the mesh and P-pressure at the corner nodes. For the uncoupled scalar transport problems any common 2D element may be chosen, linear triangles and quads are used for two of the benchmark problems discussed later.

For the sake of comparison, optional extra terms corresponding to the an SUPG (streamline-upwind Petrov-Galerkin) formulation [3, 5] formulation are added to the advection-diffusion stiffness term $\mathbf{K_T}$ of the discretised scalar transport equation 12, which adds some additional diffusion in the streamline direction (this however as part of a consistent Petrov-Galerkin approach). The 'smoothing' effect is further enhanced by a 'discontinuity capturing' term [16] in the direction of the steepest scalar gradients.

2.2 Time integration

Temporal discretisation of the time domain is achieved by applying the generalised midpoint rule, [17, 18].

$$\left[\frac{\mathbf{M}_{\mathbf{n}+\alpha}}{\alpha\Delta t}+\mathbf{K}_{\mathbf{n}+\alpha}\right](T_{n+1}) = \left[\frac{\mathbf{M}_{\mathbf{n}+\alpha}}{\alpha\Delta t}-\frac{(1-\alpha)}{\alpha}\mathbf{K}_{\mathbf{n}+\alpha}\right](T_n)+\frac{(\mathbf{F}_{\mathbf{n}+\alpha})}{\alpha} \tag{13}$$

Variation of α leads to different members of this family of methods *i.e.*

$\alpha = 0$ -Forward Difference or Forward Euler

$\alpha = \frac{1}{2}$ -Midpoint rule

$\alpha = \frac{2}{3}$ -Galerkin

$\alpha = 1$ -Backward Difference or Backward Euler

In keeping with the 'honest' GFEM theme of this paper the midpoint rule is chosen, with timestep sizes chosen to be small enough to avoid oscillations between time steps. The choice of an unconditionally stable implicit method is enforced by the use of h-adaptivity as the smallest elements determine the stability of conditionally stable explicit methods, which makes them impractical for use in this context.

3 ADAPTIVITY

The use of h-adaptivity removes the necessity of designing a suitable mesh at first and perhaps going through an expensive trial-and-error process. Adaptivity automatically produces an optimal mesh based on a user specified discretisation error thus saving computational time and focusing effort *intelligently* over successive time steps on areas of high scalar gradients (which for the problems considered here coincide with the areas of high velocity gradients). There are five distinct steps to the iterative adaptive process used here:

1. Solution of the coupled system
2. Recovery of smoothed scalar gradients using the super-convergent patch recovery (SPR) method [19]

3. Error Estimation using the *a-posteriori* error calculated at all nodes in the mesh for the scalar field

4. Mesh refinement based on the mesh sizes produced from the previous step

5. Transfer of all data to the new mesh

3.1 Recovery

The temperature field generated by the finite element method is most accurate at nodal points whereas the temperature gradients are most accurate at Gaussian integration points, known as the super-convergence phenomenon. Hinton and Campbell [20] showed that finite elements produce superior values of temperature gradient at node points after application of a *smoothing* procedure. Their method was based on a global smoothing scheme requiring the solution of a large system of equations. A more efficient and effective procedure was introduced by Zienkiewicz and Zhu [19], called super-convergent patch recovery (SPR). The smoothed nodal gradients are calculated from the Gauss points on a patch of elements surrounding a node, using a least squares interpolation, for each node in the mesh.

3.2 Error Estimation

The error estimator used was originally derived for heat conduction [21]. Mathematical justification of using such an estimator for advection-diffusion problems does not exist, however as the estimator used is based on the scalar flux, it has proven very effective in detecting regions of high scalar gradient, which in practice is sufficient for the purposes of this paper. The *a-posteriori* error is based upon an *energy norm* (see [21]),

$$||e||^2 = \int_\Omega (\nabla T)^T \kappa \nabla T d\Omega - \int_\Omega (\nabla \hat{T})^T \kappa \nabla \hat{T} d\Omega \tag{14}$$

if we define,

$$\begin{aligned} ||Q||^2 &= \int_\Omega (\nabla T)^T \kappa \nabla T d\Omega \\ ||\hat{Q}||^2 &= \int_\Omega (\nabla \hat{T})^T \kappa \nabla \hat{T} d\Omega \end{aligned} \tag{15}$$

then Equation (14) can be rewritten as

$$||e||^2 = ||Q||^2 - ||\hat{Q}||^2 \tag{16}$$

Such a definition allows a practical representation of the error norm in terms of a percentage error η,

$$\eta = \frac{||e||}{||Q||}\text{x}100\% \tag{17}$$

3.3 Mesh refinement

Specification of a permissible error $\bar{\eta}$ determines the level of refinement throughout the mesh, leading to a predicted reduction or increase in the element sizes so that the new mesh may possess an approximately equal distribution of error. The maximum permissible error for each element is calculated as,

$$||\hat{e}||_e \;=\; \bar{\eta}\left(\frac{||Q||^2}{m}\right)^{\frac{1}{2}} \tag{18}$$

where m is the number of elements, $\bar{\eta}$ is the specified maximum percentage error. Dividing $||\hat{e}||_e$ by the calculated error in an element yields a parameter ξ_e as follows,

$$\xi_e \;=\; \frac{||e||_e}{||\hat{e}||_e} \tag{19}$$

i.e. if $\xi_e > 1$ the mesh must be refined in the vicinity of element e, conversely, if $\xi_e < 1$ the mesh may be coarsened. The new element size is calculated using,

$$\bar{h_e} \;=\; \frac{h_e}{{\xi_e}^{\frac{1}{p}}} \tag{20}$$

where h_e is the original element size and p is the order of the element shape functions.

3.4 Data transfer to new mesh

Ensuring proper transfer of variables between meshes is crucial for conservation of quantities such as energy, mass and momentum. A transfer strategy using local coordinates of nodal points and

elemental shape functions has been used that maps the mesh data accurately. The local coordinates $(\xi - \eta)$ of each node in the adapted mesh are determined with respect to the elements of the previous mesh. Element shape functions are then used to interpolate the data onto the new mesh nodes.

The formulations described above have been implemented in the implicit transient FE code CADTRAS (Coupled Advective Diffusive TRAnSport model). The code incorporates an unstructured Delaunay triangulation based mesh generator [22], which allows automatic adaptive re-meshing to take place at each time step if necessitated by the error estimation algorithm.

4 BECNCHARAK EXAMPLES

A number of benchmark problems are presented in the following sections to demonstrate the method described.

4.1 Steady state pure advection

The first problem considered is one where no amount mesh refinement is able to provide a satisfactory solution without using a 'wiggle suppressent' [5, 6]. It is a classical benchmark problem for testing advective transport algorithms, where a step discontinuity at a boundary is advected into and out of a domain of regular geometry. The source of 'wiggles' in this problem is both the steepness of the 'wave form' to be advected and that it is introduced as a Dirichlet boundary condition.

For this problem the SUPG method is used (with and without the discontinuity capturing term) and the (excellent) results are shown in Figure 1. These results were achieved using an iterative adaptive scheme, four intermediate meshes from which are shown in Figure 2.

The same problem was solved using GFEM using the final adaptive mesh obtained from the SUPG solution. The result is shown in Figure 3, which clearly shows that for this problem the SUPG method or equivalent is indispensable.

4.2 Time-dependent pure advection

The second problem that of a advecting a cosine hill in a rotating velocity field, the exact solution being a rigid body rotation of the cosine hill. For this problem a few adaptive passes were executed

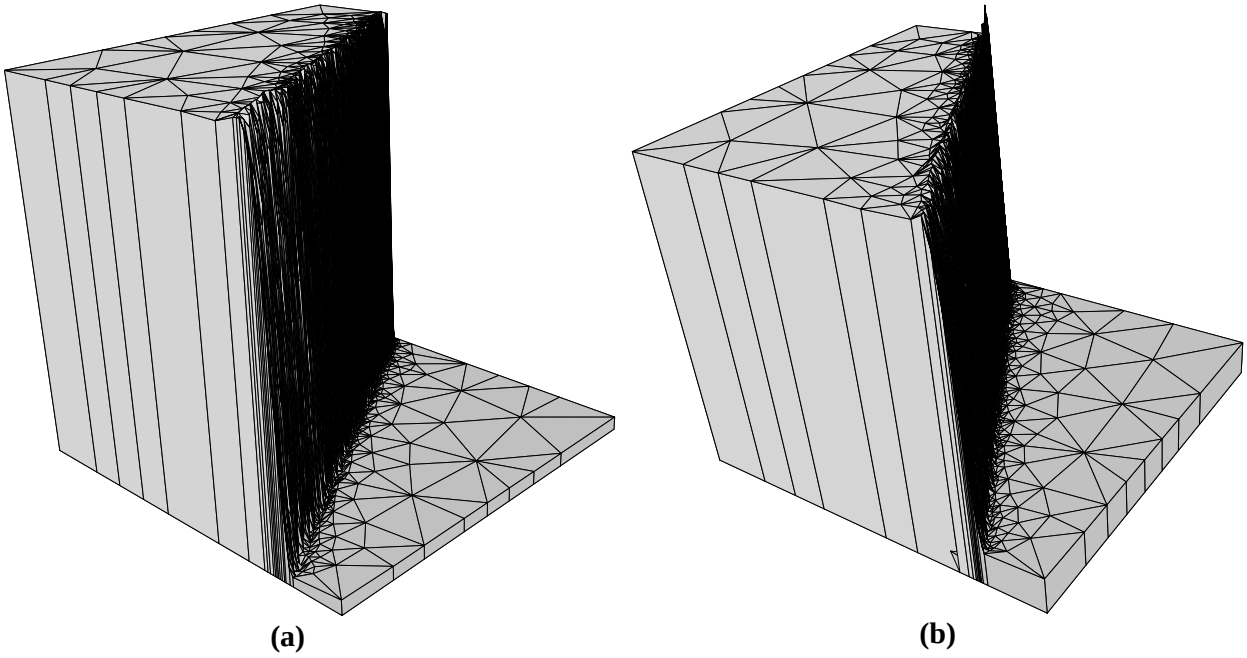

Figure 1: Adaptive solution (a)SUPG with discontinuity capturing term (b)SUPG without discontinuity capturing term

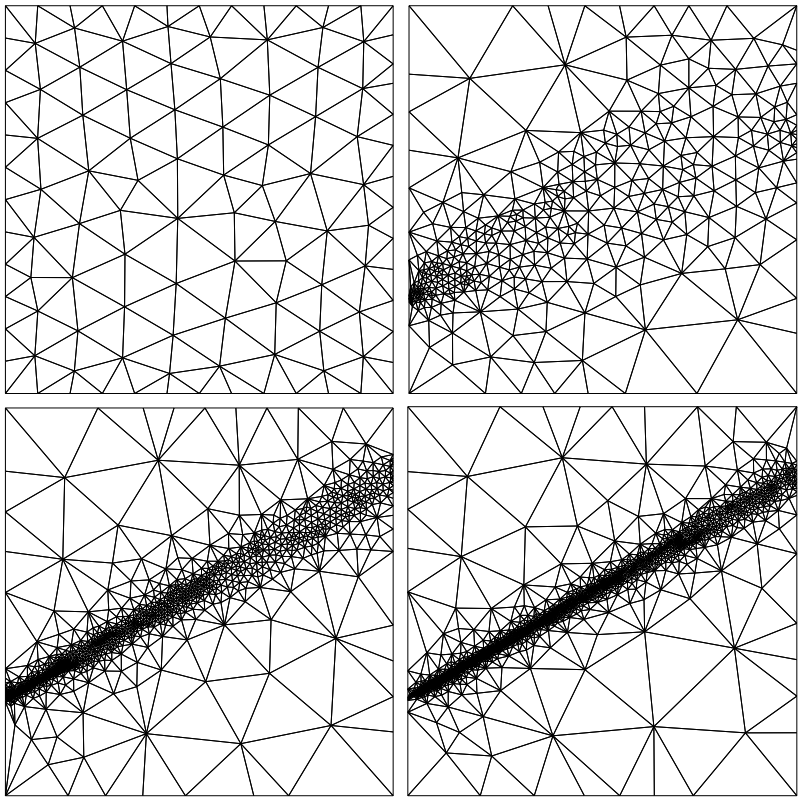

Figure 2: Sequence of selected adaptive meshes

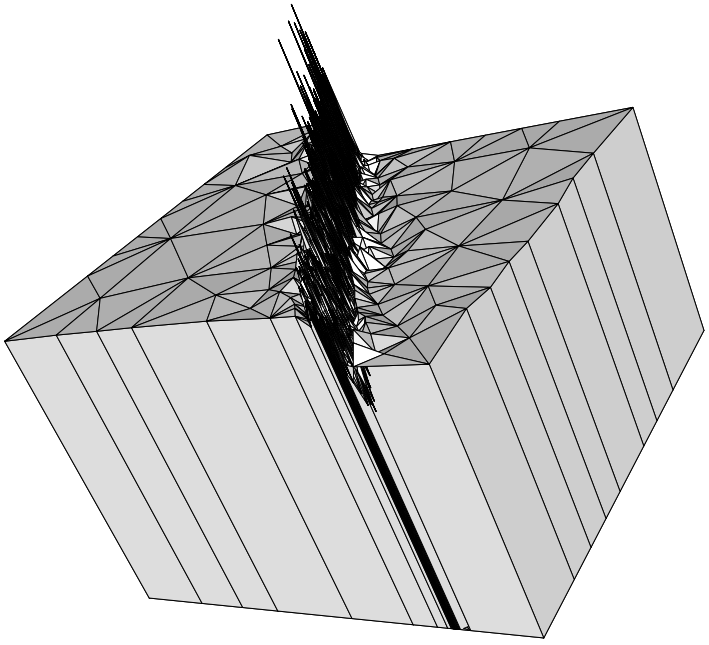

Figure 3: GFEM solution using the final adaptive mesh

on the initial conditions to obtain a suitable mesh right from the beginning of the analysis [6]. Figure 4 shows the solutions obtained after one revolution of the cosine hill, using both SUPG and GFEM. Although there is relatively larger phase error in the GFEM solution (demonstrated by the thickness of the base), the results from this problem show quite clearly that unlike the previous problem, a *wiggle suppressent* (such as SUPG) is not essential for time-dependent problems if h-adaptivity is used leading to meshes appropriate for the problem being produced automatically. Four of these meshes are shown in Figure 5.

4.3 Natural convection in a thermally driven cavity at high Rayleigh numbers

The method is further tested by application to the well documented benchmark problem of the thermally driven cavity. This problem becomes more difficult to solve at high Rayleigh numbers characterised by; thin boundary layers, separation and recirculation zones and oscillatory internal waves dominating the flow behaviour. The authors successfully benchmarked this method for Rayleigh numbers (Ra) up to 10^8 [7], when the solution reaches a steady state. Further tests were performed for even higher Ra, up to 4×10^8, for cases where no steady states exist and the solution moves from

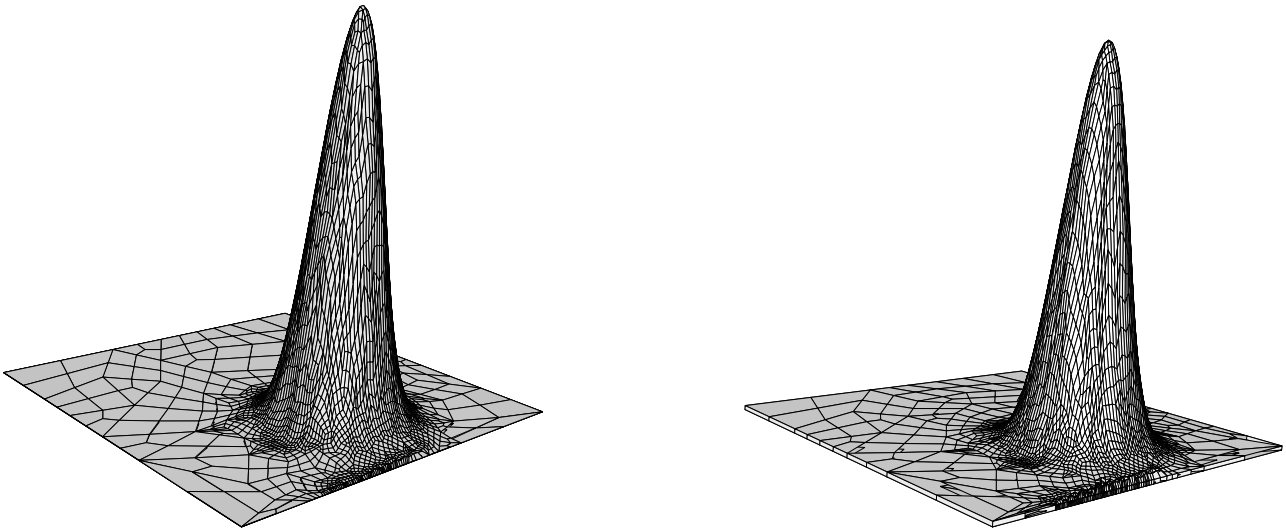

(a) SUPG Solution

(b) GFEM Solution

Figure 4: Cosine hill after one revolution using an adaptive mesh and 200 timesteps

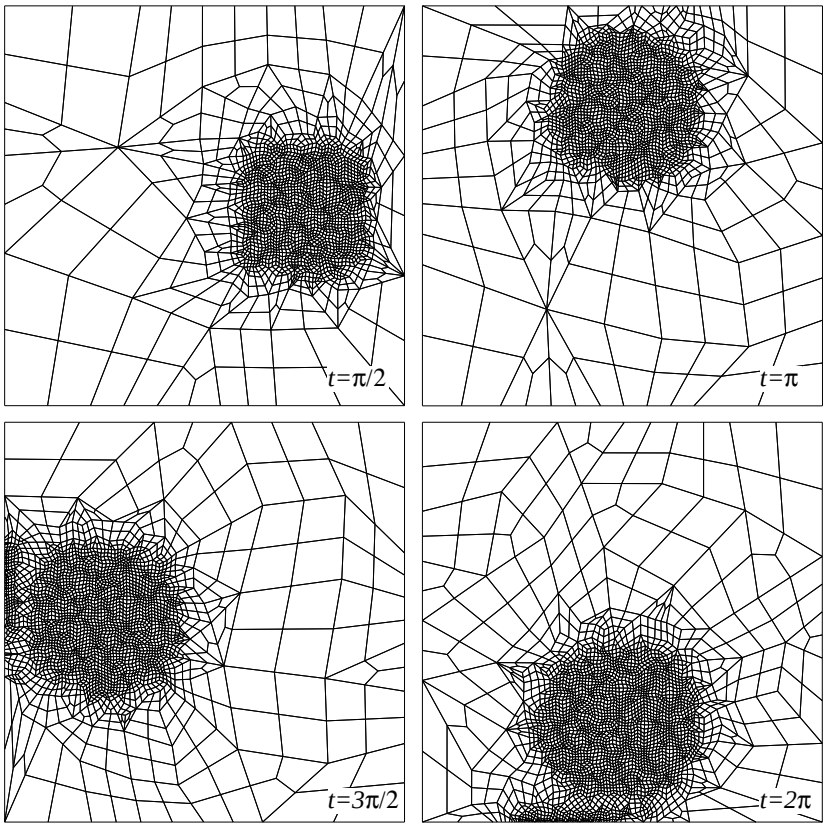

Figure 5: Adaptive meshes at quarter revolutions

periodic to quasi-periodic to mildly chaotic [8]. Figure 6 show adaptive meshes at 6 time points for the Ra $= 4 \times 10^8$ case. Figures 7 and 8 show the corresponding velocity and temperature fields. The apparent wiggles in the temperature field contours indicates that the mesh may still not be sufficiently refined (the 'self diagnostic' property of GFEM), this is because a limit to the minimum element size possible was enforced during the adaptive process. Finally, Figure 9 shows the time history of the temperature variation at the top left-hand departing corner of the square cavity (x=0.1032, y=0.8036) along with a fast-Fourier transform analysis unravel the frequency content of the solution. These results compared favourably with other published work [23].

4.4 Natural convection in a cubical air-filled cavity

This final problem was set as a 3D benchmarking exercise for the CHT'01 Conference [24]. It involves modelling fluid flow in a two dimensional square cavity of typical dimension L with the two opposing walls being maintained at a temperature difference of ΔT (see Figure 10). The temperature of the remaining walls varies linearly from T_h to T_c, set to 300 K and 307 K respectively.The velocities at all four walls are set to zero, enforcing no-slip conditions. The fluid inside the cavity is initially at rest and at a temperature which is the mean of the temperatures on the vertical walls. Fluid properties are considered to be invariant with temperature. The steady state flow and heat transfer in the thermal cavity is characterised by the Rayleigh number,

$$Ra \;=\; g\beta\frac{\Delta T L^3}{\nu\alpha} \tag{21}$$

Temperature, velocity, time and distance were non-dimensionalised as per Mayne *et al* [25].

Table 1 presents a range of Nusselt numbers for each angle and Rayleigh number examined.

$\theta = 90^o$

Solutions for Ra $= 10^6$ and 10^7 are given in table 1 and compare well to results presented in Leong *et al.* Ra $= 10^8$ problem does not reach steady state in a reasonable computational length of time. The magnitude of oscillations in the temperature field in the top left and bottom right hand corners of the cavity for Ra $= 10^8$ do not decrease over time which suggests an unsteady solution to the problem or at least a very slow progression to steady state. The same problem solved with adiabatic horizontal walls reaches steady state quite rapidly [7]. The influence of the linear temperature variation across

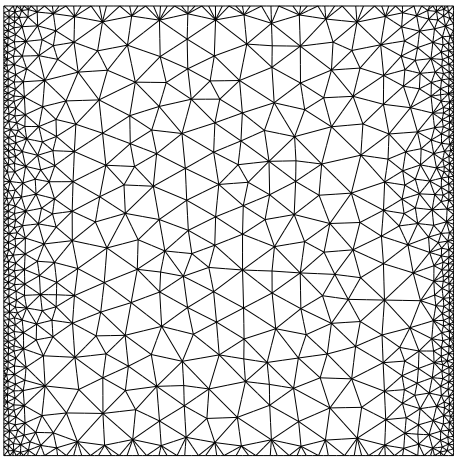

(a) Time step 1, mesh 1

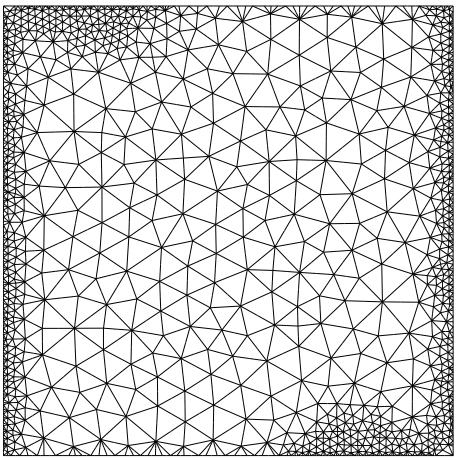

(b) Time step 14, mesh 6.

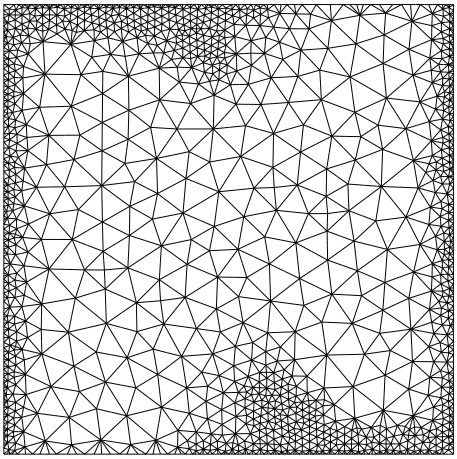

(c) Time step 22, mesh 8.

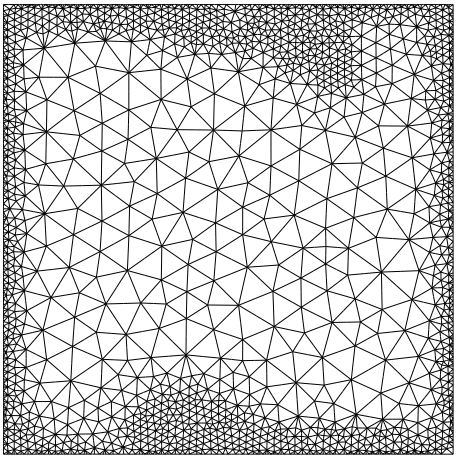

(d) Time step 33, mesh 10.

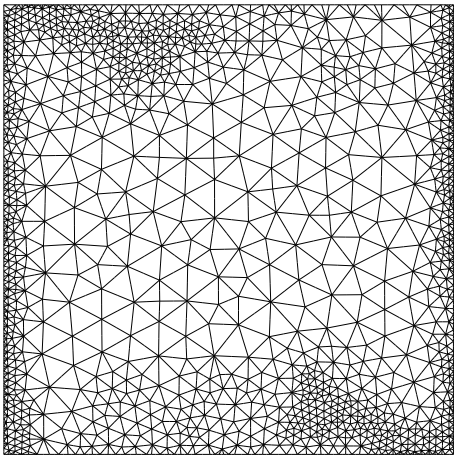

(e) Time step 69, mesh 12.

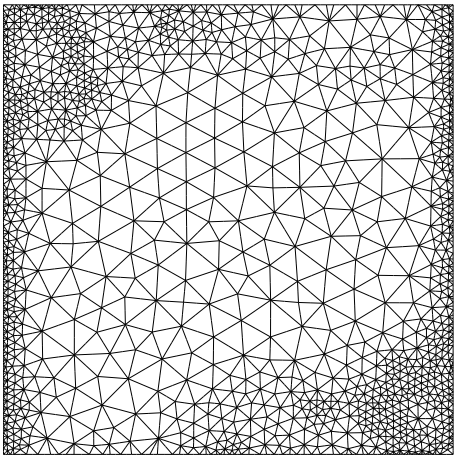

(f) Time step 78, mesh 13.

Figure 6: Adaptive mesh files for Ra $= 4 \times 10^8$ at (a) $t^* = 0.0$; (b) $t^* = 0.00028$; (c) $t^* = 0.00044$; (d) $t^* = 0.00066$; (e) $t^* = 0.00138$; (f) $t^* = 0.00156$.

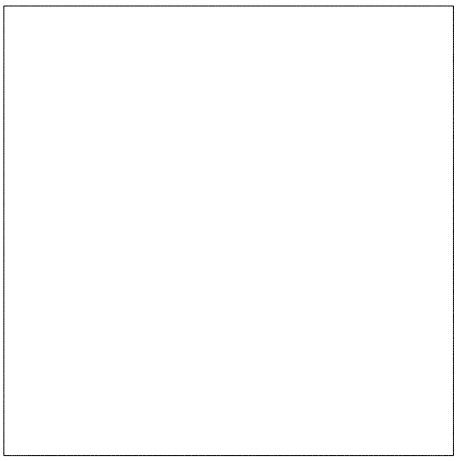

(a) Time step 1, velocity vectors.

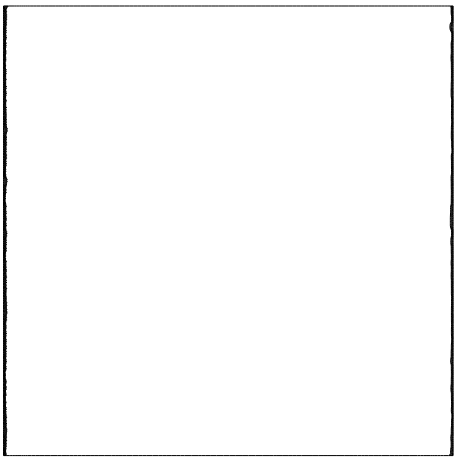

(b) Time step 1, isotherms.

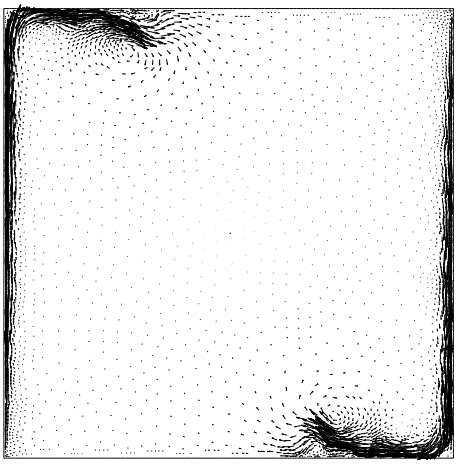

(c) Time step 14, velocity vectors.

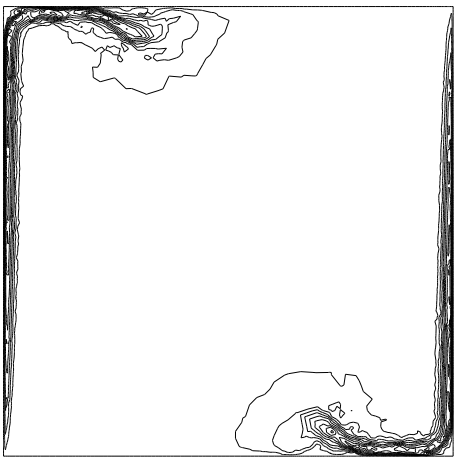

(d) Time step 14, isotherms.

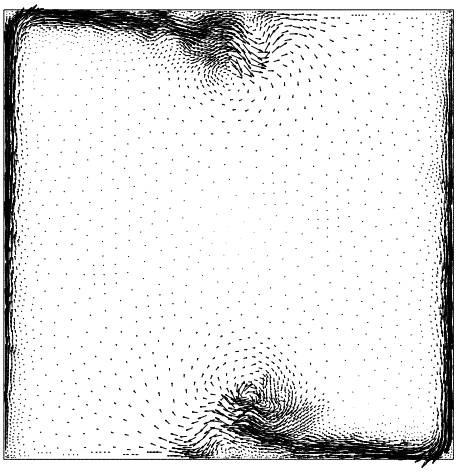

(e) Time step 22, velocity vectors.

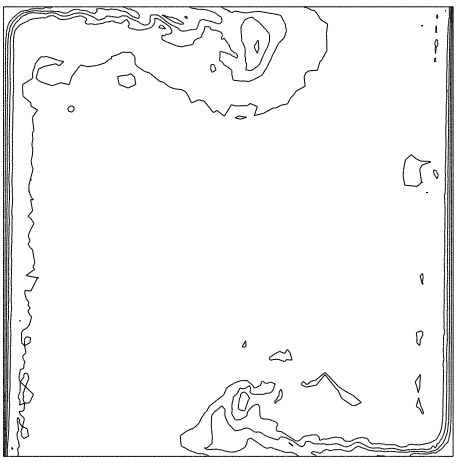

(f) Time step 22, isotherms.

Figure 7: Velocity vectors and isotherms for Ra $= 4 \times 10^8$ at (a),(b) $t^* = 0.0$; (c),(d) $t^* = 0.00028$; (e),(f) $t^* = 0.00044$.

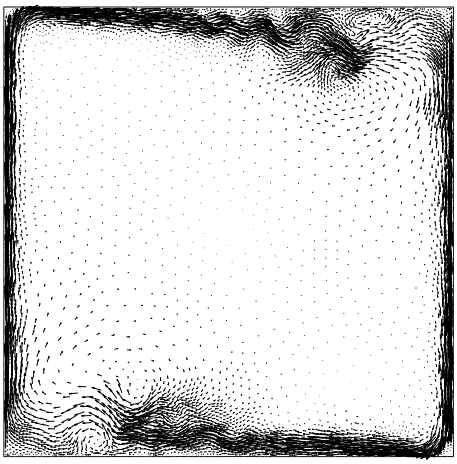

(a) Time step 33, velocity vectors.

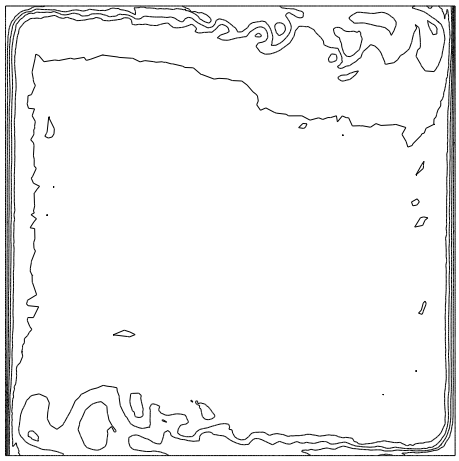

(b) Time step 33, isotherms.

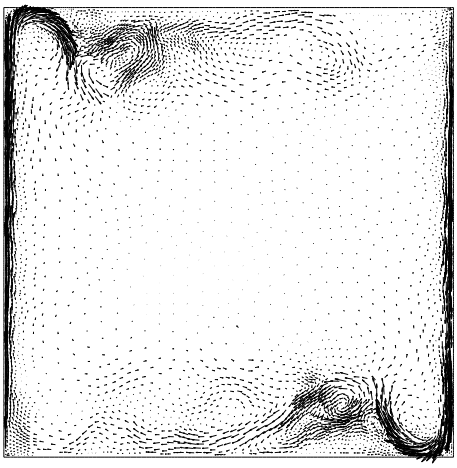

(c) Time step 69, velocity vectors.

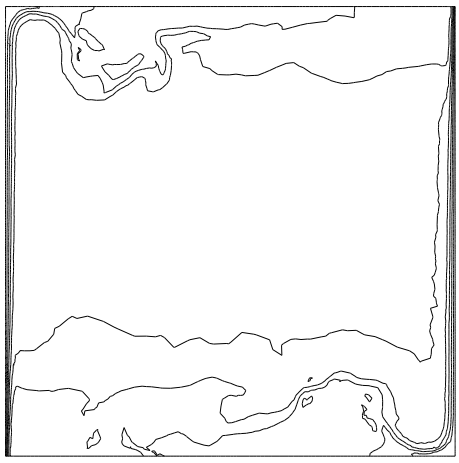

(d) Time step 69, isotherms.

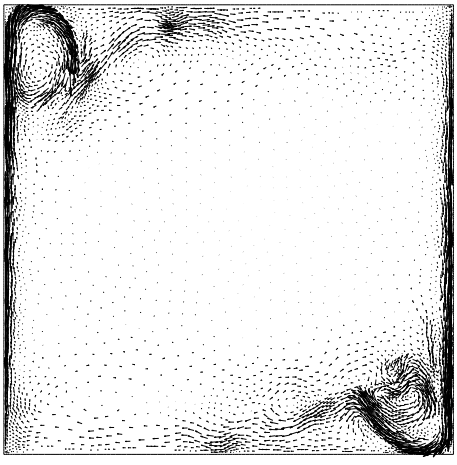

(e) Time step 78, velocity vectors.

(f) Time step 78, isotherms

Figure 8: Velocity vectors and isotherms for $\mathrm{Ra} = 4 \times 10^8$ at (a),(b) $t^* = 0.00066$; (c),(d) $t^* = 0.00138$; (e),(f) $t^* = 0.00156$.

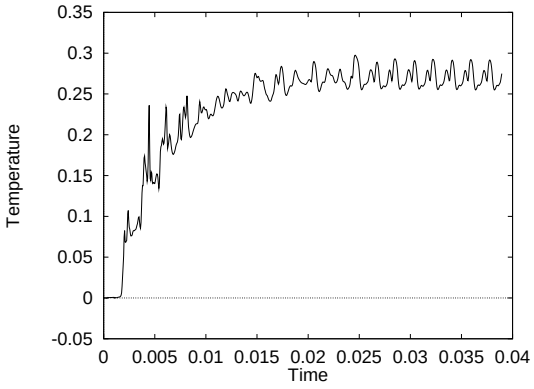

(a) Temperature, Ra $= 2 \times 10^8$

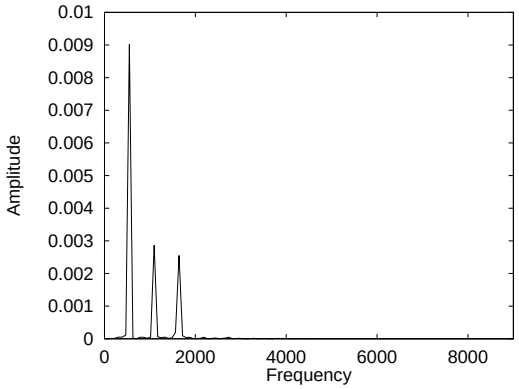

(b) FFT, Ra $= 2 \times 10^8$

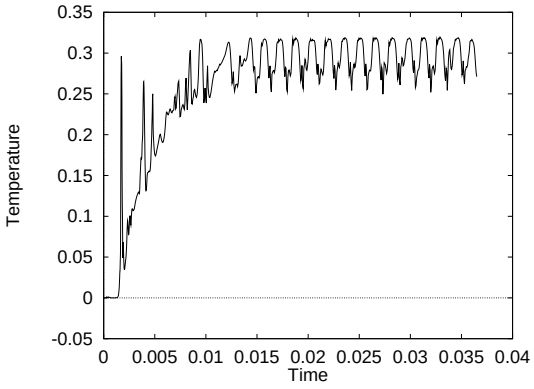

(c) Temperature, Ra $= 3 \times 10^8$

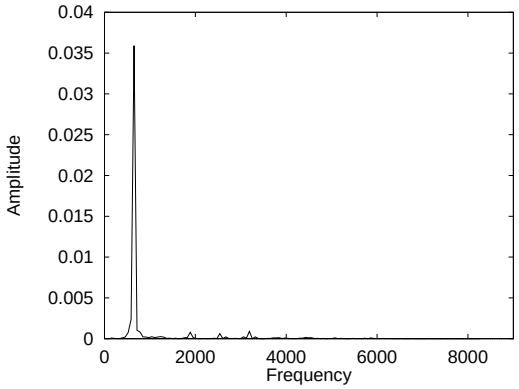

(d) FFT, Ra $= 3 \times 10^8$

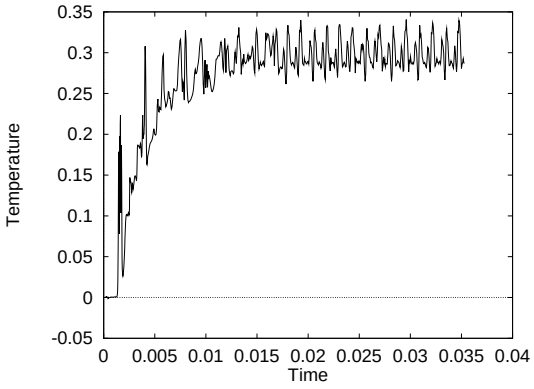

(e) Temperature, Ra $= 4 \times 10^8$

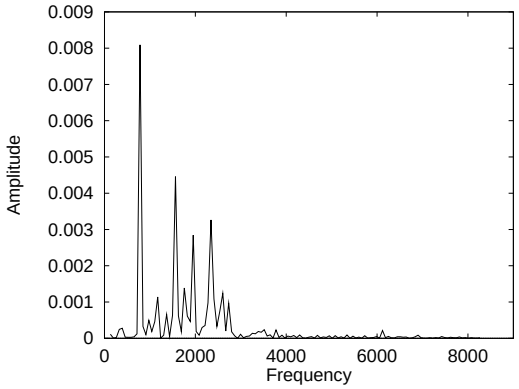

(f) FFT, Ra $= 4 \times 10^8$

Figure 9: Time trace histories and FFT plots at x = 0.1032, y = 0.8036 for temperature

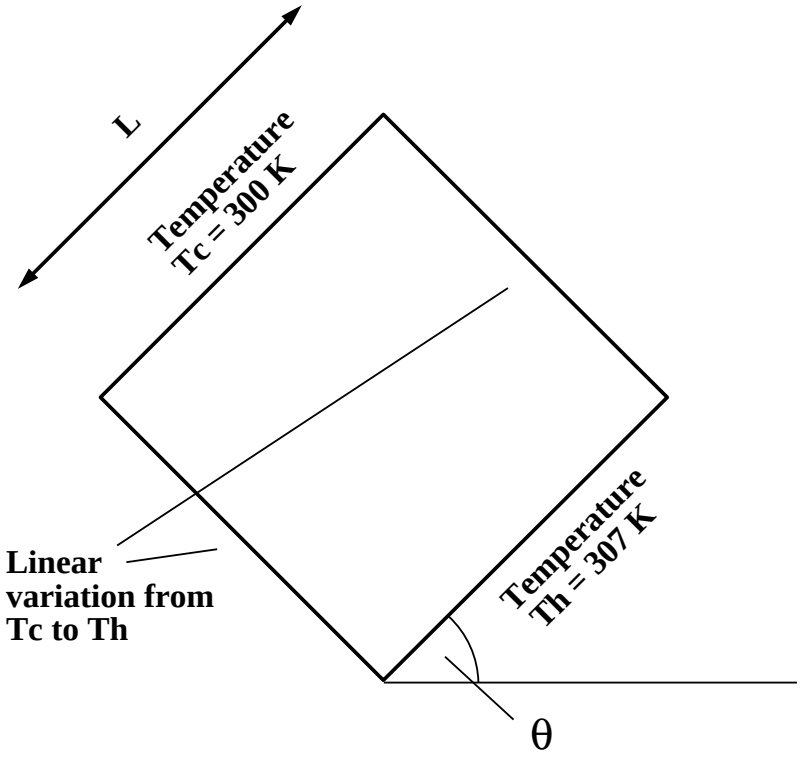

Figure 10: Boundary conditions for thermal cavity benchmark problem

the top and bottom boundaries destabilises the flow preventing a steady state solution. The absence of the third dimension in the model also removes the damping effect of the end walls in the cubic cavity, the 2-D solution assuming an infinitely wide cavity perpendicular to the plane.

$\theta = 45^o$

The average Nusselt number on the cold wall for Ra=10^6 compares well with results presented by Leong *et al* [11], coming to within 0.5 % of the experimental value. Figure 11 show the temperature and velocity fields for this case at steady state. In the solution of Ra=10^7 the progression to steady state is very slow again and a range of Nusselt number variation at the end of the analysis is given in table 1.

$\theta = 0^o$

In most of the analyses for the thermally driven cavity problem, the adaptive process reaches a stable discretisation, beyond which the mesh doesn't change any further. This happens because either the calculated errors remain below the specified maximum percentage error $\bar{\eta}$) or, the specified minimum

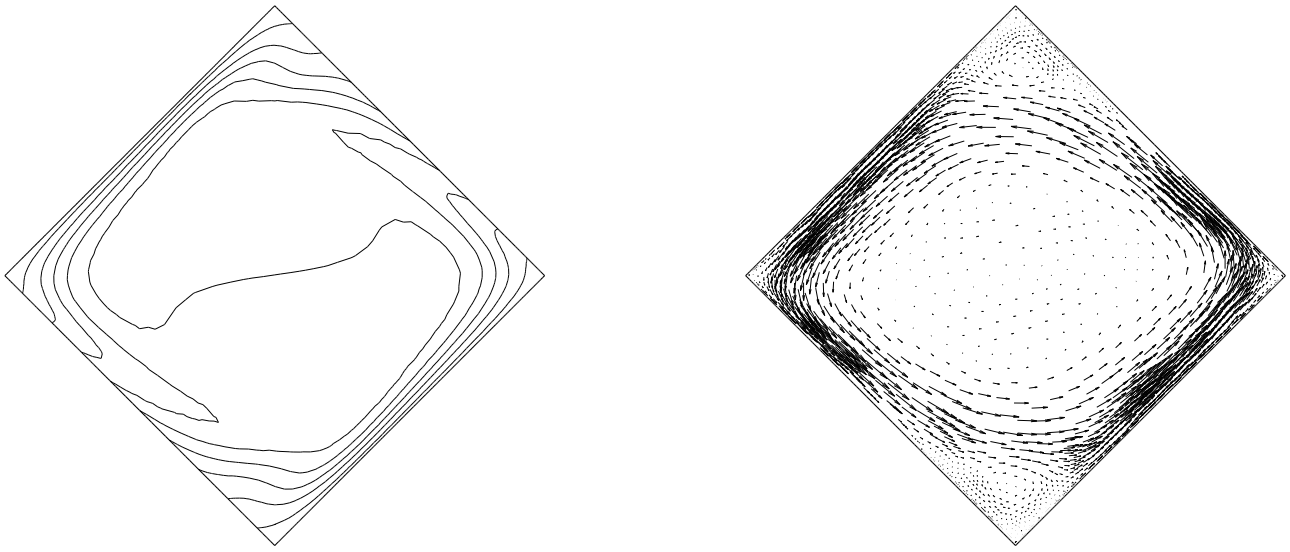

(a) Temperature field

(b) Velocity vectors

Figure 11: Steady state results for Ra=10^6

element size has been achieved by the mesh, the latter being the more likely explanantion in regions of steep gradients. Figure 12 shows the final refined mesh for the angle of 0^o and Ra=10^5. The boundary regions are highly refined, allowing effective capture of the steep temperature gradients. Figure 13 illustrates the development of isotherms and velocity vectors over time. Figure 13(a) shows the temperature distribution near the start of the run, at $t^* = 0.05439$. The isotherms are practically symmetrical in both directions, this is reflected in the velocity vectors that clearly show four identical cells, one in each corner. The equilibrium between hot and cold fronts is destabilised at $t^* = 0.08653$. This leads to hot air rising up along the left half of the domain. Figure 13(c) shows tilting in the isotherms and the beginning of a single large cell in the centre of the cavity. Finally steady state is achieved, a large central eddy dominates the flow field, two smaller re-circulations persist in the top-left and bottom right corners, see figures 13(e) and 13(f). The steady state solution for Ra = 10^5 is very different from the 3-D solution presented by Leong *et al.* The flow is clearly fully three-dimensional and cannot be modelled effectively in 2-D as stated by Kuyper *et al* [26] however the 2-D solution of this problem still generates interesting features and is worth pursuing in its own right as a benchmark for testing transient 2-D codes. The average value of Nusselt number on the cold face is lower than the experimental results. The average Nusselt number on the cold face obtained for Ra = 10^6 is also significantly below that presented by Leong *et al.*

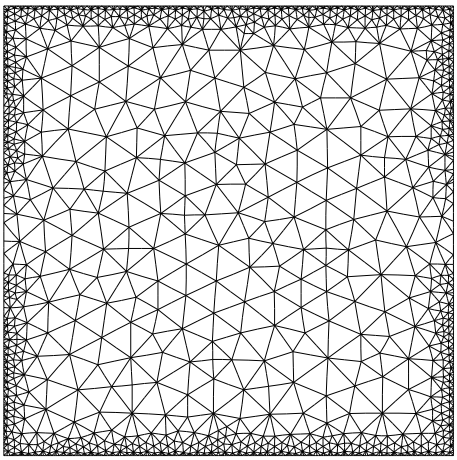

(a) Mesh, $t^* = 0.00371$

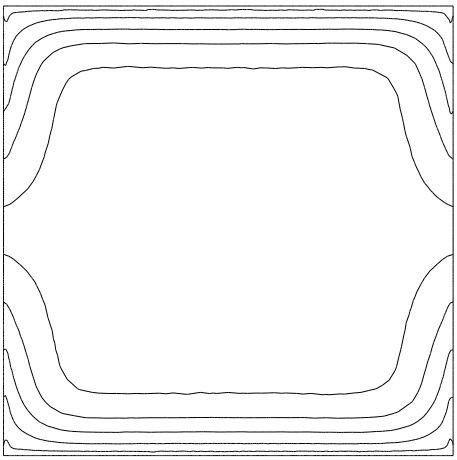

(b) Isotherms, $t^* = 0.00371$

Figure 12: Last adaptive mesh and isotherms for $\theta = 0^o$, Ra $= 10^5$

	Nu		
Ra	$\theta = 0^o$	$\theta = 45^o$	$\theta = 90^o$
10^5	2.6549	-	-
10^6	3.4214	8.8823	6.4806
10^7	-	15.3427-19.9798	12.4286
10^8	-	-	22.7993-24.1878

Table 1: Results

It is clear from the above analysis that this problem can be successfully modelled in 2-D for angles of 90^o and 45^o for the Rayleigh numbers considered, however, the flow is fully three-dimensional at $\theta = 0^o$ and 2-D modelling is not satisfactory.

5 CONCLUSIONS

The benchmark examples presented show clearly that for the time-dependent problems discretisation produced by using h-adaptivity made it unnecessary to use any special schemes and GFEM was sufficient for producing accurate and efficient solutions while maintaining its 'self diagnostic' property. The accuracy compared favourably with other published solutions. Both the spatial and temporal discretisation schemes used here have a central difference character and suffer from oscillatory behaviour

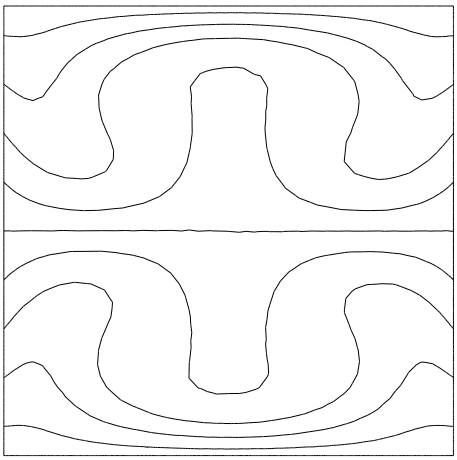

(a) Isotherms, $t^* = 0.05439$

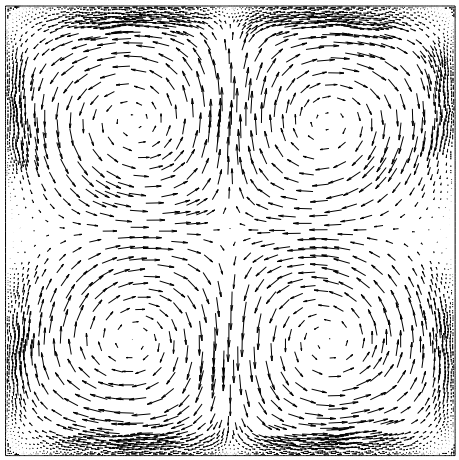

(b) Velocity vectors, $t^* = 0.05439$

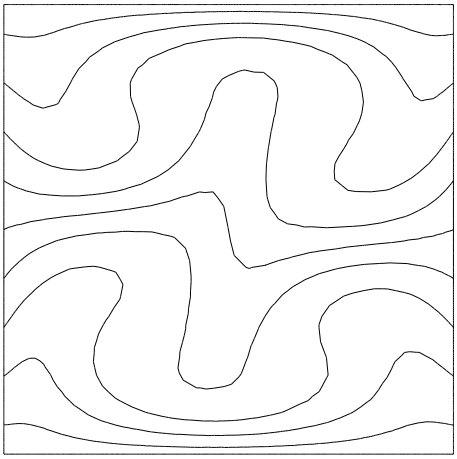

(c) Isotherms, $t^* = 0.10136$

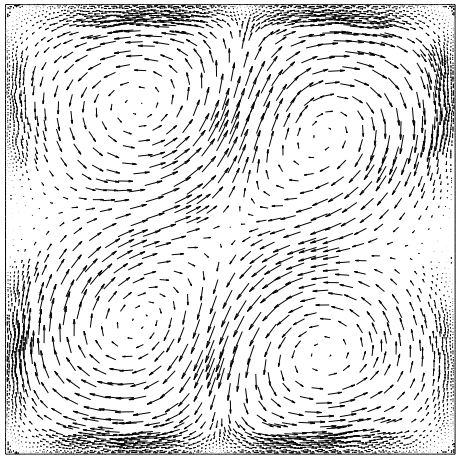

(d) Velocity vectors, $t^* = 0.10136$

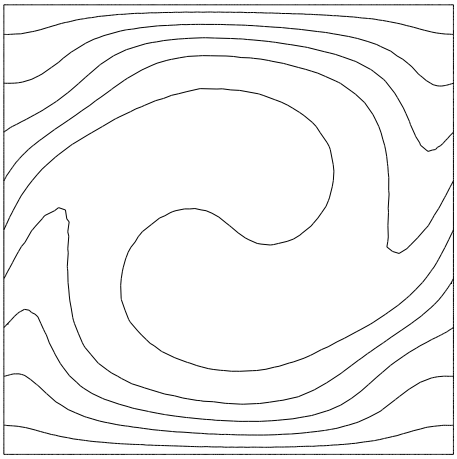

(e) Isotherms, $t^* = 0.48703$

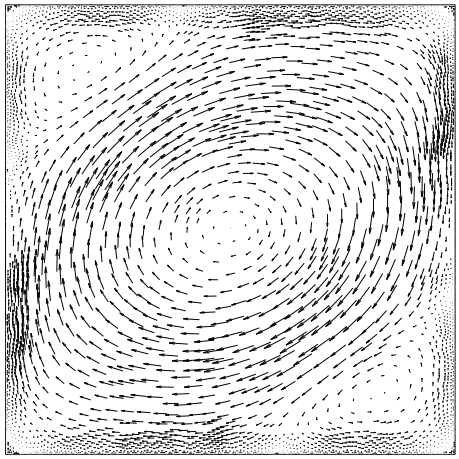

(f) Velocity vectors, $t^* = 0.48703$

Figure 13: Isotherms and velocity vectors for angle = 0^o, Ra = 10^5

in problems where sharp gradients are present, leading to the use of 'wiggle suppressent' upwinding or other higher order schemes, with uncertain results. h-adaptive methods with automatic mesh refinement based upon the actual physics of the problem are inherently efficient as no development time is required to create the 'right' mesh for a problem. They are also economical as an 'optimal' discretisation is produced for a desired level of accuracy, with grid-points placed only where they are needed. Another significant advantage in using such an approach is that relatively little additional work is required in modifying existing codes. The actual computational time is divided between the solution of the discretised governing equations and the adaptive process (gradient recovery, error-estimation and mesh refinement). The adaptive process accounted for only 0.25% of the total CPU time in the thermally driven cavity problems solved here. This can be reduced further by using simpler structured meshes with a mesh enrichment method of refinement. In solving these problems the conservation of mass was also monitored and the differences arising from data transfer from one mesh to another were within one half of a percent.

References

[1] P.M.Gresho and R.L.Sani. *Incompressible Flow and the Finite Element Method.* John Wiley and Sons, Chichester, 1998.

[2] P.M. Gresho and R.L.Lee. Don't suppress the wiggles - they are telling you something! *Computers and Fluids*, 9:223–253, 1981.

[3] A.N.Brooks and T.J.R.Hughes. Streamline upwind/petrov-galerkin formulations for convection dominated flows with particular emphasis on the incompressible navier-stokes equations. *Computer Methods in Applied Mechanics and Engineering*, 32:199–259, 1982.

[4] H.C.Huang and A.S.Usmani. *Finite Element Analysis for Heat Transfer - Theory and Software.* Springer-Verlag, London, 1994.

[5] A.S.Usmani. An h-adaptive SUPG-FEM solution of the pure advection equation. *Applied Numerical Mathematics*, 26:193–202, 1998.

[6] A.S.Usmani. Solution of steady and transient advection problems using an h-adaptive finite element method. *International Journal of Computational Fluid Dynamics*, 11:249–259, 1999.

[7] D.A.Mayne, A.S.Usmani, and M.Crapper. *h*-adaptive finite element solution of high Rayleigh number thermally driven cavity problem. *International Journal of Numerical Methods in Heat and Fluid Flow*, 10:598–615, 2000.

[8] D.A.Mayne, A.S.Usmani, and M.Crapper. *h*-adaptive finite element solution of unsteady thermally driven cavity problem. *International Journal of Numerical Methods in Heat and Fluid Flow*, 11:172–194, 2001.

[9] A.S.Usmani. Solution of advection problems using *h*-adaptive FEM with discontinuity capturing SUPG method. In *International Symposium on Advances in Computational Heat Transfer: Book of Abstracts*, pages 123–125, Cesme, Turkey, May 1997. Organised by International centre for Heat and Mass Transfer.

[10] W.H.Leong, K.G.T.Hollands, and A.P.Brunger. On a physically-realizable benchmark problem in internal natural convection. *International Journal for Heat and Mass Transfer*, 41:3817–3828, 1998.

[11] W.H.Leong, K.G.T.Hollands, and A.P.Brunger. Experimental nusselt numbers for a cubical-cavity benchmark problem in natural convection. *International Journal for Heat and Mass Transfer*, 42:1979–1989, 1999.

[12] P.M.Gresho, R.L.Lee, S.T.Chan, and R.L.Sani. Solution of the time-dependent incompressible navier-stokes and boussinesq equations using the galerkin finite element method. In *Proceedings of the IUTAM Symposium on Approximate Methods for Navier-Stokes Problems*, pages 203–222, Paderborn,West Germany, September 1979.

[13] P.M.Gresho, R.L.Lee, and R.L.Sani. On the time-dependent solution of the incompressible Navier-Stokes equations in two and three dimensions. In *Recent Advances in Numerical Methods in Fluids*, volume 1. Pineridge Press Limited, Swansea, 1980.

[14] A.S.Usmani, R.W.Lewis, and K.N.Seetharamu. Finite element modelling of natural-convection-controlled change of phase. *International Journal for Numerical Methods in Fluids*, 14:1019–1036, 1992.

[15] C.Taylor and P.Hood. A numerical solution of the navier-stokes equations using the finite element technique. *Computers and Fluids*, 1:73–100, 1973.

[16] T.J.R.Hughes, M.Mallet, and A.Mizukami. A new finite element formulation for computational fluid dynamics: II. Beyond SUPG. *Computer Methods in Applied Mechanics and Engineering*, 54:341–355, 1986.

[17] T.J.R.Hughes. Analysis of transient algorithms with particular reference to stability behaviour. In *Computational Methods for Transient Analysis*. Elsevier Science Publishers, 1983.

[18] T.J.R.Hughes. *The Finite Element Method - Linear Static and Dynamic Finite Element Analysis*. Prentice-Hall International, Inc., New Jersey, 1987.

[19] O.C.Zienkiewicz and J.Z.Zhu. Adaptivity and mesh generation. *International Journal for Numerical Methods in Engineering*, 32:783–810, 1991.

[20] E.Hinton and J.S.Campbell. Local and global smoothing of discontinuous finite element functions using a least squares method. *International Journal for Numerical Methods in Engineering*, 8:461–480, 1974.

[21] R.W.Lewis, H.C.Huang, A.S.Usmani, and J.T.Cross. Finite element analysis of heat transfer and flow problems using adaptive remeshing including application to solidification problems. *International Journal for Numerical Methods in Engineering*, 32:767–781, 1991.

[22] H.C.Huang and A.S.Usmani. *The Finite Element Analysis for Heat Transfer*. Springer-Verlag, 1994.

[23] D.R.Chenoweth and S.Paolucci. Natural convection in an enclosed vertical air layer with large horizontal temperature differences. *Journal of Fluid Mechanics*, 169:173–210, 1986.

[24] In G.de Vahl Davis and E.Leonardi, editors, *CHT'01:Advances in Computational Heat Transfer II*, Cairns, Australia, May 2001.

[25] D.A.Mayne, A.S.Usmani, and M.Crapper. h-adaptive finite element solution of high rayleigh number thermally driven cavity problem. *International Journal of Numerical Methods in Heat and Fluid flow*, 10:598–615, 2000.

[26] R.A.Kuyper, Th H. Van Der Meer, C.J.Hoogendoorn, and R.A.W.M.Henkes. Numerical study of laminar and turbulent natural convection in an inclined square cavity. *International Journal for Heat and Mass Transfer*, 36:2899–2911, 1993.